Photochemistry and Photobiology, 2001, 73(6): 636–641

Autofluorescence Microscopy of Fresh Cervical-Tissue Sections Reveals Alterations in Tissue Biochemistry with Dysplasia¶

Rebekah Drezek[1], Carrie Brookner[2], Ina Pavlova[1], Iouri Boiko[3], Anais Malpica[4], Reuben Lotan[5], Michele Follen[3,6] and Rebecca Richards-Kortum*[1]

[1]Biomedical Engineering Program and Department of Electrical and Computer Engineering, The University of Texas at Austin, Austin, TX;
[2]Ethicon Inc., Somerville, NJ;
[3]Departments of Gynecologic Oncology [4]Pathology and [5]Tumor Biology, M.D. Anderson Cancer Center, Houston, TX and [6]Department of Obstetrics, Gynecology, and Reproductive Health Sciences, The University of Texas Health Science Center, Houston, TX

Received 18 December 2000; accepted 8 March 2001

ABSTRACT

Fluorescence spectroscopy offers an effective, noninvasive approach to the detection of precancers in multiple organ sites. Clinical studies have demonstrated that fluorescence spectroscopy can provide highly sensitive, specific and cost-effective diagnosis of cervical precancers. However, the underlying biochemical mechanisms responsible for differences in the fluorescence spectra of normal and dysplastic tissue are not fully understood. We designed a study to assess the differences in autofluorescence of normal and dysplastic cervical tissue. Transverse, fresh tissue sections were prepared from colposcopically normal and abnormal biopsies in a 34-patient study. Autofluorescence images were acquired at 380 and 460 nm excitation. Results showed statistically significant increases in epithelial fluorescence intensity (arbitrary units) at 380 nm excitation in dysplastic tissue (106 ± 39) relative to normal tissue (85 ± 30). The fluorophore responsible for this increase is possibly reduced nicotinamide adenine dinucleotide. Stromal fluorescence intensities in the dysplastic samples decreased at both 380 nm (102 ± 34 [dysplasia] *vs* 151 ± 44 [normal]) and 460 nm excitation (93 ± 35 [dysplasia] *vs* 137 ± 49 [normal]), wavelengths at which collagen is excited. Decreased redox ratio (17–40% reduction) in dysplastic tissue sections, indicative of increased metabolic activity, was observed in one-third of the paired samples. These results provide valuable insight into the biological basis of the differences in fluorescence of normal and precancerous cervical tissue.

INTRODUCTION

One century ago the mortality associated with cervical cancer exceeded that of any other malignancy in U.S. women (1). Despite the introduction of screening programs based on the Papanicolaou's (Pap)† smear over the past 50 years cervical cancer still poses a significant worldwide health threat. Cervical cancer is the second most common malignancy in women today (2). More than 471 000 cases are diagnosed each year, predominantly among women in the developing countries (2). Because of the high costs of screening programs and the lack of trained health-care providers in developing areas cervical cancer often remains undetected. In the United States more than $6 billion per year is spent on treating and evaluating low-grade precursor lesions, many of which are not likely to progress to cancer. New technologies are needed to address the needs of cancer-screening and detection programs in both developed and developing nations. Ideally, these technologies would improve and automate the screening and detection process while reducing health-care costs.

Interest in the use of optical technologies to detect premalignant lesions has grown in recent years. Optical technologies offer the ability to noninvasively diagnose and monitor precancers *in vivo*. For many precancers and early cancers the current standard of care relies on histopathologic assessment of directed biopsies in order to obtain a final diagnosis. With optical technologies diagnosis can be achieved in real time, using automated techniques and without removing tissue. This reduces the required clinical expertise, reduces unnecessary biopsies and, in certain instances, permits diagnosis and treatment to be accomplished in a single visit to a health-care provider. Fluorescence spectroscopy is an emerging optical technology that offers particular

¶Posted on the website on 19 March 2001.
*To whom correspondence should be addressed at: Biomedical Engineering Program, The University of Texas at Austin, ENS 610, Austin, TX 78712, USA. Fax: 512-471-0616; e-mail: kortum@mail.utexas.edu

†*Abbreviations*: CCD, charge-coupled device; FAD, flavin adenine nucleotide; H&E, hematoxylin and eosin; HGSIL, high-grade squamous intraepithelial lesion; LGSIL, low-grade squamous intraepithelial lesion; MMP, matrix metalloproteinase; NAD, nicotinamide adenine dinucleotide; NADH, reduced nicotinamide adenine dinucleotide; Pap, Papanicolaou's; PBS, phosphate-buffered saline.

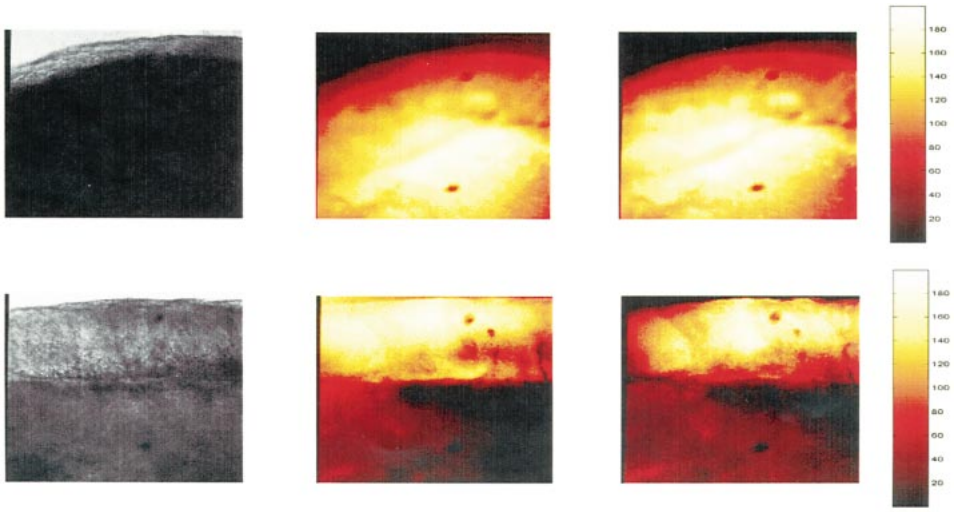

Figure 1. Representative images from paired normal and dysplastic fresh tissue sections. The top row shows images from a squamous normal biopsy; the bottom row shows images from an abnormal biopsy (pathology: LGSIL). In each row the images from left to right are as follows: brightfield image, 380 nm excitation image, 460 nm excitation image ([35 year–old]). The size of the fluorescence and brightfield images shown in all the figures is approximately 1×1 mm^2. Intensities at 380 nm excitation and 460 nm excitation are not directly comparable.

promise for the diagnosis of disease in part because of a large number of endogenous biological fluorophores. Some of the more common tissue fluorophores include the aromatic amino acids (tryptophan, tyrosine and phenylalanine), the cofactor reduced nicotinamide adenine dinucleotide (NADH), flavins, porphyrins, collagen and elastin (3). Because fluorescence spectroscopy offers a means of assessing both the structural and the biochemical progression of the disease, interest in its use to detect precancers has been increasing. Clinical studies have achieved promising results in multiple organ sites including the breast, lung, oral cavity, gastrointestinal tract and cervix (see Richards-Kortum and Sevick-Muraca [3] for a recent review of clinical studies involving fluorescence spectroscopy). Several studies have investigated the use of fluorescence spectroscopy to diagnose cervical neoplasia, including a 95-patient, *in vivo* study of cervical-tissue fluorescence excited at 337, 380 and 460 nm (4,5). A fluorescence spectroscopy–based algorithm developed to classify normal and precancerous cervical tissue in a diagnostic setting outperformed colposcopy and alternative approaches (Pap smear, cervicography and human papillomavirus testing) (6).

Although it has been shown that fluorescence spectra measured from normal and dysplastic cervical tissue show consistent differences that can be exploited for tissue diagnosis, there has been little work to elucidate the biological basis of the differences, which could provide insight valuable to improving the technique's diagnostic performance. The analysis of the spectra from cervical tissues is complicated by the tissue's distinct two-layer structure: an epithelial layer composed of several layers of cells and an underlying stroma consisting largely of structural proteins and the supporting vasculature. Some of the constituents of both the tissue layers are fluorescent, including the structural proteins collagen and elastin, found in the stroma, and the metabolic indicators NADH and flavin adenine dinucleotide (FAD), found predominantly within the mitochondria of cells.

Because the pyridine nucleotides and flavins play an integral role in cellular metabolism, it is possible to assess a tissue's metabolic status by monitoring the changes in the concentrations of these electron carriers. The reduced form of nicotinamide adenine dinucleotide (NAD), *i.e.* NADH, and the oxidized form of FAD are fluorescent, whereas the oxidized electron carrier NAD^+ is only very weakly fluorescent, and the reduced electron carrier $FADH_2$ is nonfluorescent. Thus, fluorescence measurements provide a useful method for noninvasively monitoring the changes in metabolism (7). A tissue's metabolic state is sometimes described by calculating the ''redox ratio,'' a quantity obtained by dividing the fluorescence of FAD by the sum of the fluorescences of FAD and NADH. The redox ratio, which typically decreases in cancer, is sensitive to changes in the metabolic rate and vascular oxygen supply (8).

We have investigated the use of fresh tissue sections as a model for *in vivo* cervical-tissue fluorescence and have demonstrated the feasibility of this model by imaging fluorescence from normal cervical samples (9). The fresh tissue sections are prepared using a microtome, developed by Krumdieck *et al.* (10), designed to prepare fresh tissue slices rapidly with minimal tissue trauma. Results from an initial 31-patient study showed an age-dependent pattern of autofluorescence (9). In contrast to the results obtained with frozen–thawed sections significant epithelial fluorescence was observed in the images. However, the epithelial contribution decreased with increasing patient age. Stromal fluorescence was also noted and increased with patient age. Understanding the autofluorescence patterns of normal cervical tissue provided important new data regarding the biological basis of the clinically measured spectra. In this paper we expand upon our previous work by considering the autofluorescence of paired normal and dysplastic biopsies.

The goals of the current study were two-fold: first, to use fresh tissue sections to qualitatively and quantitatively characterize the autofluorescence of normal and dysplastic cervical tissue; and second, to determine whether variations in the metabolism of normal and dysplastic tissue are evident in redox images of the tissue sections. This study demonstrates that changes in the intensity of fluorescence in both the cervical epithelium and the underlying stroma can be correlated to the presence of dysplasia. Observed differences in epithelial fluorescence are attributed to increased cellular metabolism in dysplastic tissue. The observed decrease in the intensity of stromal fluorescence in dysplastic tissue is attributed primarily to changes in the collagen biochemistry.

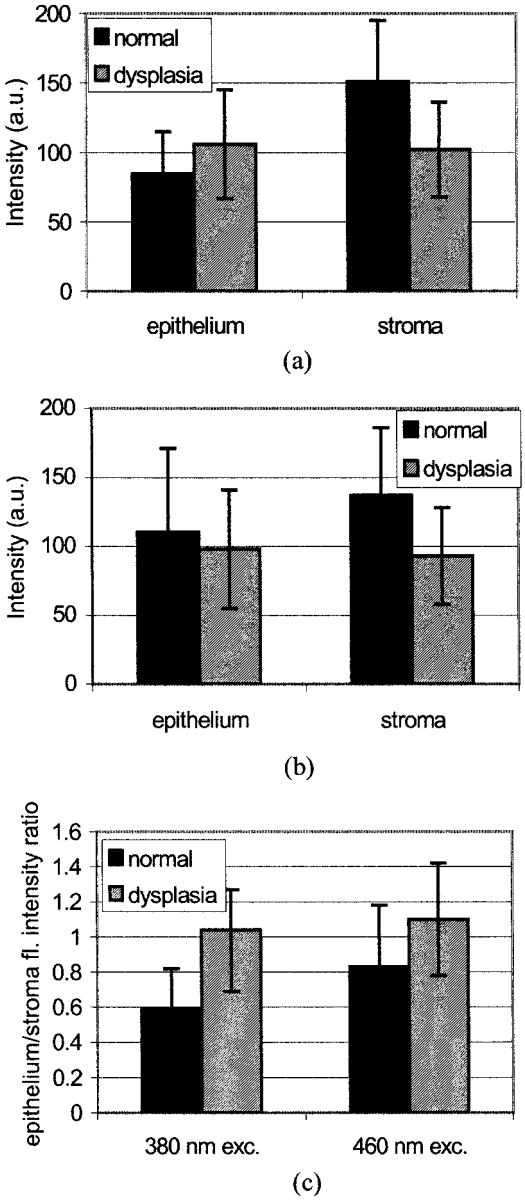

Figure 2. a: Average intensity in the epithelium (squamous normal *vs* dysplasia) and the stroma (normal *vs* dysplasia) at 380 nm. b: Average intensity in the epithelium (squamous normal *vs* dysplasia) and the stroma (normal *vs* dysplasia) at 460 nm. c: Comparison of the ratio of fluorescence intensity in the epithelium and stroma (squamous normal *vs* dysplasia) at 380 and 460 nm excitation. Error bars represent 2 SD. Intensities at 380 and 460 nm excitation are not directly comparable.

MATERIALS AND METHODS

Slice preparation. Cervical biopsies ($2 \times 4 \times 1$ mm^3) were obtained, with written consent, from women seen in The University of Texas M.D. Anderson Cancer Center Colposcopy Clinic and the Lyndon B. Johnson Hospital (LBJ) Colposcopy Clinic. These women were referred for colposcopy because of abnormal cytology or were being treated for cervical dysplasia with the loop electrosurgical excision procedure. Acetic acid (6%) was applied to the cervix of each woman during colposcopy prior to biopsy. When possible, biopsies were obtained from one colposcopically normal area and one colposcopically abnormal area. All normal biopsies were obtained from the squamous sites. The biopsies were immediately placed in chilled (4°C) culture medium (Dulbecco modified Eagle medium without phenol red) and were then embedded in 4% agarose for slicing. The Krumdieck tissue Slicer (MD1000-A1, Alabama Research and Development, Munford, AL) was used to obtain fresh tissue slices (200 μm thick) which were cut perpendicular to the epithelial surface. Fluorescence images were obtained from tissue slices within 1.5–5 h of biopsy. Control experiments showed that the fluorescence intensities varied less than 10% when imaged at a time beginning immediately following preparation and ending 5.5 h after preparation.

Fluorescence microscopy. An Axiophot 410 inverted fluorescence microscope (Carl Zeiss, Thornwood, NY) was used to examine the unstained tissue slices under brightfield and fluorescence conditions. Neofluar optics (Carl Zeiss) were used to provide high transmission for wavelengths from 360 nm. Areas with recognizable epithelium and stroma were identified under brightfield. Autofluorescence images were then collected from these areas at 380 and 460 nm excitation, using the 100 W mercury lamp of the microscope and a filter cube with filter sets I (BP380 exciter filter, FT410 dichroic mirror, 420 long-pass filter) and II (BP455 exciter filter, FT470 dichroic mirror, GG495 filter). All the filters were obtained from Omega Optical (Brattleboro, VT). The average power delivered to the tissue surface was 750 μW at 380 nm excitation and 930 μW at 460 nm excitation. The microscope was coupled to a liquid nitrogen–cooled charge-coupled device (CCD) camera (Photometrics Series 200) with 12-bit resolution and 512×512 pixels. The CCD camera was operated cooled to approximately −120°C. Image acquisition was computer controlled using the Iplab image-processing software. For each fluorescence image the appropriate dark-current image and the temperature of the camera were recorded. Corresponding brightfield images of each tissue slice were acquired over the same field as the fluorescence image. A rhodamine calibration standard was used to assess the day-to-day variations in system response.

For the biopsies from the first 17 patients the tissue slices were kept in chilled culture medium during the imaging, and an image of a field of medium was collected as a control. After the first 17 patients we altered the sample-preparation technique in order to improve image sharpness and to eliminate the need to subtract background fluorescence from the culture medium. For the remaining patients the tissue slice was removed from the culture medium immediately prior to imaging, rinsed with phosphate-buffered saline (PBS) and placed on a quartz slide. PBS was added to the slide to prevent the tissue slice from drying out. The tissue slices obtained from one biopsy were observed using both sample-preparation techniques to ensure that the change in procedure did not alter the observed fluorescence.

All the fluorescence images were collected using a 10× objective (model 440331, Carl Zeiss). The objective had a working distance of 5.6 mm and a numerical aperture of 0.3. For both wavelengths a 5 s exposure time was used in all cases except for two biopsies. For these two biopsies, a 1 s exposure time was used to avoid image saturation, and counts were scaled appropriately. A series of experiments in which slices were repeatedly imaged using a 5 s exposure was performed to confirm that photobleaching was not a concern in the obtained images. Fluorescence intensities obtained after 20 repeated 5 s exposures were approximately 90% of the intensity measured after a single 5 s exposure.

Image analysis. For slices imaged in culture medium the background fluorescence of the medium was subtracted from each fluorescence image. For the remainder of the slices the appropriate dark-current image was subtracted from each fluorescence image. An average intensity of fluorescence from the epithelium and fluorescence from the stroma was calculated for each image. Large rectangular regions were chosen to cover as much of the epithelium or stroma as possible while avoiding features in the images such as holes. The boundaries of the epithelial and stromal layers were determined by comparing the fluorescence images to the corresponding brightfield images and, when necessary, to the matching histology slides. No image areas without tissue were included. The average intensities in the epithelium and stroma and their ratio (epithelium/stroma) were calculated for each image. To enhance the visualization of tissue fluorescence in the images presented in this paper, pseudocolor was added after the image analysis was completed.

Tissue metabolism. Redox images were created for the imaged slices by dividing the 460 nm excitation image by the sum of the

380 and 460 nm excitation images. Correction factors based on the rhodamine standard were used to account for the wavelength-dependent features of the excitation portion of the experimental setup. Correction factors for the emission path were calculated using measured transmission curves for the dichroic mirror and long-pass filter and the quantum efficiency curve provided by the camera's manufacturer. Pseudocolor was added to enhance visualization.

Histological staining. Following fluorescence microscopy the tissue slices were fixed in 10% formalin, embedded in paraffin, and 4 μm sections were made for histological evaluation. A standard hematoxylin and eosin (H&E) protocol was used to stain the sections from each tissue slice. The stained sections were used to correlate the fluorescent areas to the histological features of the tissue. A pathologist with expertise in gynecologic pathology, who was blinded to the fluorescence images, read the H&E slides and provided a diagnosis of the particular tissue imaged (I.B., A.M.).

RESULTS

Thirty-four patients were enrolled in the study. The patients ranged from 21 to 61 years in age (mean patient age was 33 ± 11 years). Because of the fresh tissue's fragility and the tendency of the epithelium to become detached from the stroma, in particular for the dysplastic samples, the process used to create fresh tissue sections was not always successful. For 20 patients both colposcopically normal and colposcopically abnormal biopsies were obtained, sliced and successfully imaged. In an additional six patients either the colposcopically normal or the colposcopically abnormal biopsy was sliced and imaged. In the remaining eight patients neither the normal nor the abnormal biopsy was successfully sliced and imaged. After imaging the slices H&E were created using standard techniques. In some cases the intact tissue slices did not survive the H&E-generation process. In 17 patients with both colposcopically normal and colposcopically abnormal biopsies H&E of both biopsies were made. In 12 of these 17 patients the clinical impression at colposcopy was confirmed histologically for both the normal and the abnormal tissue. Of the 12 patients with histologically confirmed normal and abnormal tissue slices seven patients had low-grade squamous intraepithelial lesions (LGSIL) and five patients had high-grade squamous intraepithelial lesions (HGSIL). Among the five patients for whom the colposcopic impression did not match the histologic findings, the tissue which appeared abnormal at the time of colposcopy was later classified as either inflammation (three patients) or normal (two patients) upon histopathologic examination. In this study normal tissue is defined as tissue classified pathologically as squamous normal or inflammation. Abnormal tissue included both LGSIL and HGSIL.

Figure 1 shows representative images of the most common pattern of fluorescence observed when comparing squamous normal and dysplastic tissue from the same patient. The size of the fluorescence and brightfield images shown in the figures throughout this paper is approximately 1×1 mm^2. In these images it is evident that fluorescence intensity increases in the epithelium of the dysplastic tissue relative to the normal tissue, whereas the fluorescence in the stroma significantly decreases. When the brightfield and fluorescence images of the squamous normal biopsy are compared it is apparent that the top portion of the epithelium in the normal tissue is almost totally nonfluorescent. In the bottom third of the epithelium in the abnormal biopsy, a region of histologically confirmed dysplasia, the fluorescence is brighter in portions of the 380 nm image relative to the corresponding 460 nm image. It should be noted that epithelial fluorescence patterns may vary significantly from patient to patient. A detailed study of the epithelial fluorescence patterns of normal cervical tissue is described by Brookner *et al.* (9).

After the intensity data (in arbitrary units) were quantified for all the paired biopsies the normality of the data was assessed with normal quantile–quantile plots and the Shapiro–Wilk statistic. The assumption of normality was accepted. The average epithelial fluorescence and average stromal fluorescence of the normal and abnormal paired data at 380 nm excitation are shown in Fig. 2a. The average epithelial fluorescence was increased in the dysplastic samples (106 ± 39) relative to the normal samples (85 ± 30). The means were found to be statistically different using a paired two-tailed Student's *t*-test ($P < 0.025$). In contrast, the average stromal fluorescence was markedly reduced in the dysplastic samples (102 ± 34) relative to the normal samples (151 ± 44). Between the normal and the abnormal groups the intensities of fluorescence in the stroma were statistically different ($P < 0.001$ using a paired two-tailed Student's *t*-test).

Figure 2b shows the same samples as Fig. 2a but at 460 nm excitation. At 460 nm excitation the average epithelial fluorescence was slightly decreased in the dysplastic samples (98 ± 43) relative to the normal samples (110 ± 61) but not in a statistically significant manner. The average stromal fluorescence was reduced in the dysplastic samples (93 ± 35) relative to the normal samples (137 ± 49). Between the normal and the abnormal groups the intensities of fluorescence in the stroma were statistically different ($P < 0.005$ using a paired two-tailed Student's *t*-test).

The ratio of the mean epithelial fluorescence to the mean stromal fluorescence was computed for all the paired samples at 380 and 460 nm excitation (Fig. 2c). For 380 nm excitation the average ratios were found to be 0.59 ± 0.23 and 1.04 ± 0.23 for the normal and the abnormal samples, respectively. Using a paired Student's *t*-test these ratios were found to be statistically different ($P < 0.002$). For 460 nm excitation the average ratios were found to be 0.83 ± 0.35 and 1.10 ± 0.32 for the normal and the abnormal samples, respectively. Using a paired Student's *t*-test these ratios were found to be statistically different ($P < 0.05$).

To determine whether the fluorescence images might contain evidence of metabolic changes between normal and dysplastic tissue we calculated redox images by dividing the 460 nm excitation image by the sum of the 380 and 460 nm excitation images. Figure 3 shows examples of redox images obtained from two patients. In both cases the redox ratio is fairly constant throughout the epithelium of the normal tissue, while significant decreases in redox ratios are seen in the regions of the image corresponding to dysplasia. The dysplasia begins in the basal layers of the epithelium, and the changes in redox are apparent here. Marked changes in redox in the dysplastic tissue were observed in one-third of the paired samples. In these cases the redox ratios in the regions of dysplasia (~0.1–0.2) were 17–40% of the average epithelial redox ratio of squamous normal tissue (~0.3–0.6). Redox ratios were calculated only over the dysplastic and

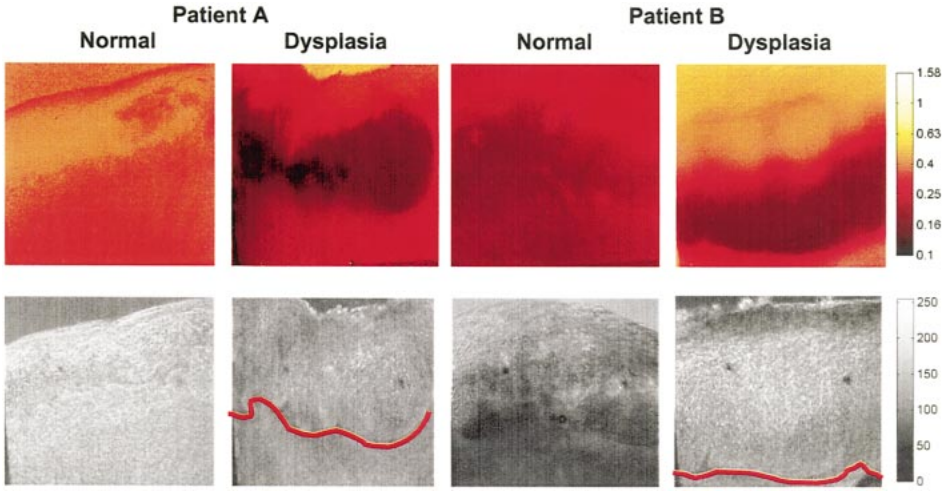

Figure 3. Representative redox images from two patients. Upper row from left to right: patient A—redox image of squamous normal tissue, redox image of dysplastic tissue (pathology: LGSIL); patient B—redox image of squamous normal tissue, redox image of dysplastic tissue (pathology: LGSIL). Lower row: brightfield images for each corresponding redox image above. Red lines indicate approximate position of the basement membrane in brightfield images.

corresponding normal regions of the tissue and are not mean redox ratios for the entire epithelium.

DISCUSSION

Fluorescence spectroscopy may provide a clinically valuable tool for the detection of precancers; however, the full potential of this technique will not be realized without a more sophisticated understanding of the relationship between the underlying tissue biochemistry and fluorescence spectra measured *in vivo.* In this paper we demonstrate that fresh tissue sections can provide a valuable model system for investigating the autofluorescence patterns of normal and dysplastic cervical tissue.

In this study significant epithelial fluorescence was observed in most of the fresh tissue sections, and the fluorescence intensity increased at 380 nm excitation in dysplastic samples relative to normal samples from the same patient. Bright epithelial fluorescence was also observed in a previous 31-patient study of normal cervical tissue (9). NADH is likely to be the source of this epithelial fluorescence. Supporting this hypothesis the fluorescence measurements of ectocervical cells from primary cultures and two cervical cancer cell lines showed fluorescence consistent with NADH (9). Presuming that NADH is the dominant epithelial fluorophore at 380 nm excitation the increased NADH fluorescence found in the dysplastic tissue suggests a higher metabolic rate in the areas of dysplasia. This would create an increased concentration in the reduced electron carrier NADH and a decreased concentration in the oxidized electron carrier FAD (11). An increase in NADH fluorescence, apparent in the 380 nm excitation images, would be expected to be coupled with a reduction in FAD fluorescence, seen in the 460 nm excitation images. In this study the mean epithelial fluorescence intensity for 460 nm excitation was reduced in the dysplastic samples; however, the difference was not statistically significant.

Significant reduction in the stromal fluorescence was observed for both 380 and 460 nm excitation in the dysplastic tissue relative to the paired normal tissue. The stromal fluorescence is attributed primarily to collagen because the amount of elastin in the cervical tissue of nonpregnant women is nearly two orders of magnitude smaller than the amount of collagen (12). The fluorescence of the stroma appears to be influenced by the presence of dysplasia in the epithelium before invasion of the stroma has occurred. This suggests that some form of epithelial–stromal communication is occurring (13) and that autofluorescence may provide a novel means of studying this communication. It is known that neoplastic cells cultured in collagen I express matrix metalloproteinases (MMP) (14) and that MMP are involved in the breakdown of the extracellular matrix (15). Furthermore, immunohistochemistry and *in situ* hybridization studies have shown that significantly elevated levels of MMP-9 expression accompany cervical intraepithelial neoplasia (16). Our data demonstrates significant decrease in stromal fluorescence in dysplastic samples, and it is known that collagen fluorescence arises from crosslinks (17). We speculate that MMP released from the epithelial cells may break down the collagen crosslinks causing the collagen matrix to appear less fluorescent. We are currently conducting the necessary experiments to test this hypothesis. Increased blood volume due to neovasculature could also play a role in the decreased stromal fluorescence observed. However, because the slices are only 200 μm thick and are maintained in culture medium until the time of imaging, we do not believe that the measured stromal fluorescence intensities are significantly impacted by hemoglobin absorption.

Our results are in contrast to data collected in previous studies performed with frozen–thawed tissue. In a study of the frozen–thawed sections of cervical tissue at 380 nm excitation Mahadevan (18) found that the epithelium exhibited little autofluorescence. Lohmann *et al.* (19) also imaged transverse cryosections of cervical tissue using 340–380 nm excitation and reported that neither normal nor dysplastic tissue exhibited significant fluorescence from the epithelial layer. It is likely that the frozen–thawed tissue does not provide a realistic model of *in vivo* fluorescence. The redox state may be altered by the oxidation that occurs during cryosectioning or microscopic examination, causing NADH to be oxidized to NAD+ which is nonfluorescent. Although our results are not consistent with the fluorescence patterns observed in frozen–thawed tissue, they do directly support the predictions of two previous inverse-modeling studies based on fluorescence spectra measured *in vivo.* These studies found that NADH fluorescence increased and collagen fluorescence decreased as normal tissue became precancerous (20) or cancerous (21).

Our findings suggest that there is clinically relevant information in the fluorescence patterns of the two distinct layers of the cervix. Current fiber-optic probe designs used in clinical systems interrogate tissue volumes comprising both epithelial and stromal tissue. Our results suggest that clinically measured decreases in bulk fluorescence emission, as tissue becomes dysplastic, are partially explained by decreased collagen fluorescence in the stroma, which is modulated by a simultaneous increase in epithelial fluorescence. Although studies have demonstrated that algorithms can be developed to separate the spectra from normal and precancerous tissue with sensitivity exceeding current detection methods (4,5), discrimination between normal and abnormal spectra could be significantly improved if it were possible to decouple the epithelial and stromal fluorescence signals. This could be achieved either by developing mathematical techniques to extract separately NADH and collagen signals from measured tissue spectra or by designing fiber-optic light delivery and collection geometries to probe individually the different layers of cervical tissue. Either of these two approaches has the potential to increase markedly the diagnostic performance of *in vivo* fluorescence spectroscopy for the detection of precancers.

In conclusion, we believe that improvements in the diagnostic capabilities of fluorescence spectroscopy will depend on an improved understanding of the relationship between the tissue biochemistry and morphology and the fluorescence spectra measured *in vivo*. A more detailed and accurate model of the interaction between light and tissue, including the important fluorophores, their distribution in the tissue and the changes in fluorescence which occur during disease progression, should permit more rational device design and the development of algorithms with improved performance. Because fluorescence spectra measured *in vivo* are strongly affected by scattering and absorption within the tissue, it is difficult to ascertain the location, quantity and identity of tissue fluorophores directly from the measured spectra. Instead, a model system that accurately represents the *in vivo* fluorescence patterns, while minimizing the distortion caused by tissue scattering and absorption, is required. Fresh tissue sections provide a valuable experimental system for fundamental investigations into the differences in fluorescence patterns in normal and dysplastic tissue. Such investigations should ultimately lead to improvements in performance vital to the clinical implementation of fluorescence spectroscopy. In addition, the discovery that dysplasia is associated with significant alterations in collagen fluorescence suggests that monitoring the native fluorescence signal from collagen may provide a novel and nondestructive means of exploring the biochemical changes in the stromal extracellular matrix prior to invasion. Although this study has concentrated on applications to the cervix, the types of studies described in this paper are readily extended to other organ sites.

Acknowledgements—We acknowledge the contributions of Dafna Lotan, Kathy Nolan, Paula Genik, Judy Sandella, Alma Sbach and Andrea Edwards in the collection and preparation of specimens and assistance with data analysis. Financial support from the National Cancer Institute (PO1-CA82710) is gratefully acknowledged.

REFERENCES

1. Callahan, T. L., A. Caughey and L. Heffner (1998) *Blueprints in Obstetrics and Gynecology*. Blackwell Science, Malden.
2. NIH(1996) NIH Consensus Development Statement Online, 1–3 April [cited (2000), 1 December], Vol. 43, pp. 1–38.
3. Richards-Kortum, R. and E. Sevick-Muraca (1996) Quantitative optical spectroscopy for tissue diagnosis. *Annu. Rev. Phys. Chem.* **47**, 555–606.
4. Ramanujam, N., M. F. Mitchell, A. Mahadevan, S. Thomsen, A. Malpica, T. Wright, N. Atkinson and R. Richards-Kortum (1996) Spectroscopic diagnosis of cervical intraepithelial neoplasia (CIN) *in vivo* using laser induced fluorescence spectra at multiple excitation wavelengths. *Lasers Surg. Med.* **19**, 63–74.
5. Ramanujam, N., M. F. Mitchell, A. Mahadevan-Jansen, S. Thomsen, G. Staerkel, A. Malpica, T. Wright, N. Atkinson and R. Richards-Kortum (1996) Cervical precancer detection using multivariate statistical algorithm based on laser-induced fluorescence spectra at multiple excitation wavelengths. *Photochem. Photobiol.* **64**, 720–735.
6. Mitchell, M., S. Cantor, C. Brookner, U. Utzinger, D. Schottenfeld and R. Richards-Kortum (1999) Screening for squamous intraepithelial lesions with fluorescence spectroscopy. *Obstet. Gynecol.* **94**, 889–896.
7. Chance, B. and B. Thorell (1959) Localization and kinetics of reduced pyridine nucleotide in living cells by microfluorometry. *Biol. Chem.* **234**, 3044–3050.
8. Gulledge, C. J. and M. S. Dewhirst (1996) Tissue oxygenation: a matter of supply and demand. *Anticancer Res.* **16**, 741–750.
9. Brookner, C. K., M. Follen, I. Boiko, J. Galvan, S. Thomsen, A. Malpica, S. Suzuki, R. Lotan and R. Richards-Kortum (2000) Autofluorescence patterns in short-term cultures of normal cervical tissue. *Photochem. Photobiol.* **71**, 730–736.
10. Krumdieck, C. L., J. Ernesto Dos Santos and K. Ho (1980) A new instrument for the rapid preparation of tissue slices. *Anal. Biochem.* **104**, 118–123.
11. Chance, B. (1989) Metabolic heterogeneities in rapidly metabolizing tissues. *J. Appl. Cardiol.* **4**, 207–221.
12. Leppert, P., S. Keller, J. Cerreta, Y. Hosannah and I. Mandl (1983) Content of elastin in the human cervix. *J. Biochem. Biophys.* **222**, 53–58.
13. Ki Hong, W. and M. Sporn (1997) Recent advances in chemoprevention of cancer. *Science* **278**, 1073–1077.
14. Gilles, C., M. Polette, M. Seiki, P. Birembaut and E. W. Thompson (1997) Implication of collagen type I-induced membrane-type 1-matrix metalloproteinase expression and matrix metalloproteinase-2 activation in the metastatic progression of breast carcinoma. *Lab. Invest.* **76**, 651–660.
15. Nagase, H. and J. Woessner (1999) . Matrix metalloproteinases. *J. Biol. Chem.* **74**, 21 491–21 493.
16. Davidson, B., I. Golberg, J. Kopolovic, L. Lerner-Geva, W. Gotlieb, B. Weis, G. Ben-Baruch and R. Reich (1999) Expression of matrix metalloproteinase-9 in squamous cell carcinoma of the uterine cervix—clinicopathologic study using immunohistochemistry and mRNA *in situ* hybridization. *Gynecol. Oncol.* **72**, 380–386.
17. Akiba, K. and N. Nakamura (1977) Isolation and characterization of fluorescent material in bovine Achilles tendon collagen. *Biochem. Biophys. Res. Commun.* **76**, 1124–1129.
18. Mahadevan, A. (1998) Fluorescence and Raman spectroscopy for diagnosis of cervical precancers. Thesis, The University of Texas at Austin, Austin, TX.
19. Lohmann, W., J. Mussman, C. Lohmann and W. Kunzel (1989) Native fluorescence of unstained cryo-sections of the cervix uteri compared with histological observation. *Naturwissenschaften* **96**, 125–127.
20. Ramanujam, N., M. F. Mitchell, A. Mahadevan, S. Thomsen, A. Malpica, T. C. Wright, N. Atkinson and R. Richards-Kortum (1994) *In vivo* diagnosis of cervical intraepithelial neoplasia (CIN) using 337 nm laser induced fluorescence. *Proc. Natl. Acad. Sci. USA* **91**, 10 193–10 197.
21. Schomaker, K. T., J. K. Frisoli, C. C. Compton, T. J. Flotte, J. M. Richter, N. S. Nishioka and T. F. Deutsch (1992) Ultraviolet laser-induced fluorescence of colonic tissue: basic biology and diagnostic potential. *Lasers Surg. Med.* **12**, 63–78.